

## Caltech Faint Galaxy Redshift Survey VII: Data Analysis Techniques and Redshifts in the Field J0053+1234<sup>1</sup>

Judith G. Cohen<sup>2</sup>, David W. Hogg<sup>3,4,5</sup> Michael A. Pahre<sup>2,5,6</sup> Roger Blandford<sup>3</sup>, Patrick L. Shopbell<sup>2</sup> & Kevin Richberg<sup>2</sup>

### ABSTRACT

We present the techniques used to determine redshifts and to characterize the spectra of objects in the Caltech Faint Galaxy Redshift Survey in terms of spectral classes and redshift quality classes. These are then applied to spectra from an investigation of a complete sample of objects with  $K_s < 20$  mag in a 2 by 7.3 arcmin<sup>2</sup> field at J005325+1234. Redshifts were successfully obtained for 163 of the 195 objects in the sample; these redshifts lie in the range [0.173, 1.44] and have a median of 0.58 (excluding 24 Galactic stars). The sample includes two broad lined AGNs and one QSO.

*Subject headings:* cosmology: observations — galaxies: distances and redshifts — surveys

### 1. Introduction

The Caltech Faint Galaxy Redshift Survey, (henceforth CFGRS), is designed to measure the properties of field galaxies in the redshift interval  $0.3 \lesssim z \lesssim 1.3$ . It uses complete samples to a fixed limiting magnitude in a particular bandpass within a small solid angle on the sky. Spectra are obtained for every object in the sample with the Low Resolution Imaging Spectrograph

---

<sup>1</sup>Based in large part on observations obtained at the W.M. Keck Observatory, which is operated jointly by the California Institute of Technology and the University of California

<sup>2</sup>Palomar Observatory, Mail Stop 105-24, California Institute of Technology, Pasadena, CA 91125

<sup>3</sup>Theoretical Astrophysics, California Institute of Technology, Mail Stop 130-33, Pasadena, CA 91125

<sup>4</sup>Current Address: Institute for Advanced Study, Olden Lane, Princeton, NJ 08540

<sup>5</sup>Hubble Fellow

<sup>6</sup>Current Address: Harvard-Smithsonian Center for Astrophysics, 60 Garden St., Mail Stop 20, Cambridge, MA 02138

(henceforth LRIS) (Oke *et al.* 1995) on the 10 m Keck Telescope. The defining features of this program that distinguish it from existing and ongoing or planned surveys, such as the CfA1 Survey (Huchra *et al.* 1983), the Las Campanas Redshift Survey (Shectman *et al.* 1996), the Canada-France Redshift Survey (henceforth CFRS; Lilly *et al.* 1995a,b), the Autofib survey (Ellis *et al.* 1996), the Century Survey (Geller *et al.* 1997), the ESO slice survey (Vettolani *et al.* 1997), the Sloan Digital Sky Survey (Gunn & Knapp 1993), the Deep Survey planned by the Lick group (Koo 1998) and the 2dF Survey (Colless & Boyle 1998), are that it is possible to reach to fainter magnitudes ( $K \sim 20$  mag,  $R \sim 24$  mag) and that completeness is emphasized rather than sparse sampling over a large field. The closest counterpart to this approach is the work of Cowie *et al.* (1996), although we note that the present survey covers a larger solid angle at the survey limit. See Koo & Kron (1992) and Ellis (1997) for reviews of the subject.

There are four limitations to “pencil beam” redshift surveys of the type described in the present paper when addressing issues of galaxy evolution. The first is that the faintest fluxes at which sources can be observed in a complete redshift survey are still over four magnitudes brighter than the fluxes of the faintest detectable sources in imaging data. The second is that the total number of sources and total sky area are both limited by available telescope time because the faintest possible sources are being studied. This is particularly relevant to attempts to characterize large scale structure. The third is that it is difficult to measure spectroscopic redshifts in the range  $1.3 < z < 2.3$ —the lower limit is set by the [O II] line at  $3727\text{\AA}$  moving out of the optical regime, the upper limit by when Ly $\alpha$  enters it. This may be a crucial period in the formation and evolution of normal galaxies (Madau, Pozzetti, & Dickinson 1998). The final limitation is the difficulty of generalizing the observed properties in a small field (which may contain unique features) to the properties of the field galaxy population as a whole.

This paper presents spectroscopic results from one field located at J005325+1234, the central region of which is part of the Medium Deep Survey (Griffiths *et al.* 1994) and among the deepest fields imaged with HST prior to the Hubble Deep Field. The field measures  $2 \times 7.3$  arcmin<sup>2</sup> with a statistical sample containing 195 infrared-selected objects complete to  $K = 20$  mag, of which 24 are spectroscopically confirmed Galactic stars and 32 cannot be assigned spectroscopic redshifts. (21 of these have spectra). There are 13 additional objects with redshifts (including two more stars) that are just outside the field boundary or are within the field but too faint.

This paper is structured as follows. The sample is defined in §2, which is followed by a description of the spectroscopic observations and redshift determinations in §3. The galaxy spectra are assigned to spectroscopic and quality classes, a procedure discussed in §4.

## 2. Sample Definition

The sample, defined in Pahre *et al.* (1998), is selected by the criteria that  $K_s < 20$  mag within a  $2 \times 7.3$  arcmin<sup>2</sup> field centered at 00 53 23.20 +12 33 58 (J2000). In an effort to cut

down the thermal background of the standard Johnson  $K$  filter, which has a central wavelength  $2.2\mu\text{m}$  and FWHM  $0.4\mu\text{m}$ , there are at least two non-standard filters in this same atmospheric window in common use: the  $K'$  filter of Wainscoat & Cowie (1992) and the  $K_s$  ( $K$ -short) filter of Persson (private communication) and Skrutskie *et al.* (1999). The latter is used here, and covers at half maximum transmission the wavelength range  $2.00 < \lambda < 2.32\mu\text{m}$ . Throughout this series of papers, unless otherwise specified, we use  $K$  (denoting the standard Johnson filter) and  $K_s$  (denoting the  $K$ -short filter) interchangeably, although the appropriate  $K_s$  transmission curve is used when deriving the  $k$ -corrections in Cohen et al (1998).

This sample contains 195 objects, and we refer to this as the “main” sample. It includes 24 spectroscopically confirmed Galactic stars. The remaining 171 objects constitute the “galaxy” sample. We were able to assign redshifts to 139 of these galaxies and this is the “redshift” sample. Redshifts were also obtained for several objects that either had  $K > 20$  mag or lie just outside the boundary of the sample. A few objects which are very faint at both  $R$  and  $K$  turned up serendipitously in slitlets intended for nearby brighter objects. Adding these 13 additional objects to the main sample defines the “total” sample of 208.

The photometric data of Pahre *et al.* (1998) are already corrected for reddening by the ISM in the Galaxy. The variation in  $E(B - V)$  across the small field of our survey is insignificant. As is conventional, we ignore reddening internal to the galaxies themselves and from the IGM.

### 3. Redshift Determinations

#### 3.1. Data Acquisition and Reduction

The objects in this sample were observed using the LRIS at the Keck Observatory beginning in October 1994 and ending in January 1998. The LRIS detector is a  $2048 \times 2048$  pixel Tektronix CCD. Its dual amplifier readout mode was normally used to save time. Observations were carried out even when the weather was not photometric. Fifteen slit masks were used. Each mask has 25 to 33 slitlets and many objects were observed more than once. A few of the brightest galaxies were selected as aids to align the masks, and hence were observed many times.

Except for the last three masks (the 1997 and 1998 data), the 300 g/mm grating was used with 1.1 arcsec wide slits. This produces a scale of  $2.46 \text{ \AA}/\text{pixel}$  and a resolution of  $10\text{\AA}$ . (This is  $\sim 4$  times higher spectral resolution than that of the CFRS.) The spectral coverage is  $\sim 5000\text{\AA}$ , with the central wavelength depending on the location of the object on the sky with respect to the centerline of the slitmask as well as on the grating tilt. Two 3000 sec exposures were obtained for each of these masks.

The last three masks, containing most of the faintest objects in the sample, were observed with the 155 g/mm grating with 1.0 arcsec wide slits giving a spectral resolution of  $20\text{\AA}$ . Two or three 1800 sec exposures were obtained for each of these slitmasks. Each of these lower dispersion

spectra was slightly shifted in central wavelength (i.e., dithered spectrally between exposures). This forces a more complex reduction, but better signal-to-noise spectra are achieved. Full spectral coverage from the UV through  $10,000\text{\AA}$  is achieved with this grating for essentially all objects at the price of lower dispersion.

These multi-slit spectra were reduced in a standard way. The bias (actually right and left amplifier bias levels) was subtracted. Then, the relevant pieces were cut out of each of the multi-slit spectra for a particular object (and out of the flat field calibration exposure), cosmic rays were removed, the subsets were flattened and the bowing of the spectra (the S-distortion) was removed. When necessary, the distortion in the vertical direction along the slit which manifests itself as tilted night sky lines was also removed.

The night sky lines within the spectra themselves were used to define the wavelength scale; a third order polynomial fit is sufficient. This means in effect that there are no “arc” lines bluer than  $5199\text{\AA}$ . Sometimes that night sky emission line could not be detected, in which case  $5577\text{\AA}$  became the bluest night sky line. Sky subtraction was accomplished by fitting a second order polynomial to a range of pixels above and below the object spectrum. Linear fits were used when necessary, particularly when the object was near the top or bottom edge of the slitlet.

The spectra were reduced by JGC using Figaro (Shortridge 1988) scripts and about 20% were also done by DWH using IRAF<sup>7</sup> scripts. JGC measured all the redshifts uniformly, including remeasurement and in some cases rereduction of the spectra done by DWH as well. The redshifts were measured by visually determining the wavelengths of spectral features from plots of the spectra over various wavelength ranges on an interactive display. The assignment of rest wavelengths to the observed spectral features was straightforward for the brighter objects and for those objects with strong emission lines, but became more difficult for the faint objects showing only absorption line spectra.

While a manual redshift determination may seem outmoded in light of more automatic techniques such as that developed by Glazebrook, Offer, & Deeley (1998) for the 2dF or that of Kurtz & Mink (1998) for the CfA surveys, in this situation it is more appropriate. Here the objects are very faint relative to the background sky, the SNR is low, the sky subtraction is difficult, the exposures are long (thus increasing the number of cosmic ray hits), and most importantly we do not fully understand what features to expect in the spectra of such faint and distant galaxies. Construction of a set of templates for a machine based redshift search from (or even for) this data set would be impossible.

The spectra have been fluxed using long slit observations of standard stars from Oke (1990) taken with the same LRIS configuration as was used for the multi-slits. The absolute scale

---

<sup>7</sup>IRAF is distributed by the National Optical Astronomy Observatories, which is operated by the Association of Universities for Research in Astronomy, Inc. (AURA) under cooperative agreement with the National Science Foundation.

of a fluxed spectrum should be regarded with caution, as the nights were not all photometric, there are substantial slit losses for the more extended objects, and slitmask alignment causes an additional light loss which is variable from mask to mask and from object to object on a given mask. However, the *shape* of the continuum for a particular object should be more or less correct, and is often quite useful.

### 3.2. Redshift Measurements

Redshifts were measured for each object in each of the slitmasks. Records were also kept of the results for any serendipitous objects that fell onto slits for other targeted galaxies. At the end, the results were compiled, and the very small number of objects with multiple observations that showed discrepancies were studied more carefully to resolve them. This involved summing all the spectra together, examining the wavelength range of each of the spectra, etc.

The most difficult cases involved objects that show no emission features, but only absorption lines which do not correspond to the standard pattern of Balmer lines, H+K Ca II doublet, etc. seen in the region of the 4000Å break. Since the 4000Å region is redshifted into the strong night sky emission lines redward of the optical bandpass for  $z > 1$ , it was suspected that for such objects  $z > 1$ . To deal with these particular cases, the spectra were compared directly with spectra of high redshift galaxies (Cowie, Hu, & Songaila 1995; Steidel *et al.* 1996), the sum of spectra of absorption line galaxies in a cluster at  $z = 1.50$  kindly supplied by J. B. Oke, as well as the sums of spectra of galaxies in the higher redshift peaks in the present sample. The library of mean ultraviolet spectral energy distributions for stellar groups from IUE spectra (Fanelli *et al.* 1992) and those of model galaxies from the grid of Bruzual & Charlot (1993) were also examined.

The absorption features in the spectra of many of those objects suspected to be at  $z > 1$  are real and repeatable. The uncertainty in the redshifts is because of limited knowledge of this spectral region (for which the 2800Å region is shifted into the optical) and lack of confidence when there are only two certain features in a spectrum, both absorption lines, as to what the correct identification should be. A good example is D0K42 (which has  $R_{obs} = 23.12$ ,  $R - K = 5.14$ ), which could have either  $z = 0.54$  or the final adopted value of  $z = 1.14$  depending on whether the identification assigned to the strongest absorption features is H+K of Ca II or 2800+2850Å (Mg II+Mg I). In this case, the spectral energy distribution of the fluxed spectra and the absence of a 4000Å jump in the  $z = 0.54$  case were considered to be persuasive evidence for the higher value.

The composite quasar spectrum of Francis *et al.* (1991) provided a template for line identification in the broad emission line objects.

### 3.3. Quality Classes

We assign a quality class to the redshift of each object to give an indication of the associated uncertainty. Table 1 lists the quality classes (0 through 9) with a brief description of each. Objects with multiple features are assigned quality class 1 – 3 redshifts, depending upon the security of the redshift. Centroiding uncertainties for high SNR spectra are generally considered to be less than  $0.1 \times \text{FWHM}$ , but with the lower SNR prevalent here, we adopt a FWHM as a more appropriate uncertainty. (The uncertainty from the wavelength fit itself using the night sky lines is small by comparison.) For a feature at  $6000\text{\AA}$  with  $z < 1.5$ , a 2 pixel error with the 300 g/mm grating corresponds to a redshift uncertainty  $\leq 0.002$ .

Single emission line spectra are placed in classes 4,5. The emission line is always assumed to be  $3727\text{\AA}$  [O II]. The CFRS has adopted a similar strategy (Lilly *et al.* 1995b), although their situation is more complex as they are more likely to have confusion between  $3727\text{\AA}$  emission and  $\text{H}\alpha$  emission due to the preponderance of lower redshift galaxies in the CFRS. In our case, with our relatively broad spectral coverage, the absence of  $\text{H}\beta$  or  $4959\text{\AA}$  emission serves to rule out the possibility that a single emission line is  $5007\text{\AA}$  of [O III]. It cannot be  $\text{H}\alpha$  for lines that appear at wavelengths bluer than the rest wavelength of  $\text{H}\alpha$ , while for redder lines, one would then expect to see  $\text{H}\beta$  or the  $5007\text{\AA}$  [O III] line in emission. The only other serious possibility consistent with the absence of features in optical spectra with broad spectral coverage is  $\text{Ly}\alpha$ ; this is a serious possibility for some of the faintest objects in the sample, particularly the serendipitous ones, where only a single emission line from a very faint object falls by chance onto our slit, cf. Dey *et al.* (1998). In such cases, broad band colors might be used to look for breaks or UV dropouts, although we have chosen to assign redshifts on the basis of spectroscopy alone. The presence of a few high redshift objects in our sample should not affect our conclusions which are restricted to the properties of galaxies with  $z < 1.5$ .

Objects showing a single break, assumed to be the  $4000\text{\AA}$  break, are assigned quality class 8. Again this is a conservative choice, since at a modest redshift well within the range covered by our survey, the break just to the red of the Mg II doublet at  $2800\text{\AA}$  will lie in the optical. There are only two objects in this class in the total sample. Quality class 9 is for objects showing a single strong absorption feature which, because of the shape of the continuum, we interpret as Mg II+Mg I at  $2800+2850\text{\AA}$  rather than as Ca H+K. There are only three such objects.

Quality class 0 is for objects with very low signal and no redshift.

For future reference, the term “high quality redshifts” refers to those with a quality class indicating a secure  $z$ , specifically quality classes 1, 2, 4, or 6.

To demonstrate that the quality class 1 spectra (which comprise more than 50% of the extragalactic objects) actually do have the precision claimed above, Figure 1 shows the values of  $\sigma$  calculated from multiple spectra of a single object where each individual measurement has a quality 1 rating as a function of  $R$  magnitude. Only the galaxies with multiple spectra among the

60 brightest objects in the sample were used. There are four or more spectra for three of these galaxies.

#### 4. Galaxy Spectroscopic Classifications

A simple spectral classification was used (Table 2). “ $\mathcal{E}$ ” (emission) denotes an galaxy where the emission lines dominate the spectrum, while the few extreme starburst galaxies that could be identified are denoted by “ $\mathcal{B}$ ”. In the subsequent discussion, these two classes are usually referred to collectively as “ $\mathcal{E}$ ” (emission) galaxies. “ $\mathcal{A}$ ” (absorption) denotes an object where no emission lines are detected, while “ $\mathcal{C}$ ” (composite) is an intermediate case where both emission and absorption (usually 3727 and H+K) are seen. When both 3727 and 5007Å emission lines are present, the object is denoted “ $\mathcal{E}$ ”, or, if the absorption spectrum is also visible, “ $\mathcal{EC}$ ”. The three AGN are designated “ $\mathcal{Q}$ ”. In addition, stars are classified according to the presence or absence of TiO bands (and/or CaH bands, for M subdwarfs) as “ $\mathcal{M}$ ” or “ $\mathcal{S}$ ” and, although there are no examples in the present sample, as “ $\mathcal{W}$ ” for white dwarfs.

The assignment of a spectral class to a galaxy will depend on its redshift and on the wavelength range covered by the observations. For example, a galaxy at low redshift with strong emission at 3727 and 5007Å will be classified as “ $\mathcal{E}$ ”, but the same object if seen at  $z \sim 1.3$  when the 2800Å region is observed in the optical will show no apparent emission features and will be listed as “ $\mathcal{A}$ ”. This is particularly true for objects where the spectral coverage of the data did not extend to  $\lambda > 7500\text{Å}$ . We emphasize that for  $z < 0.9$ , an “ $\mathcal{A}$ ” galaxy is an object that has a spectrum similar to that of local elliptical galaxies. But at higher redshift, only the strongest emission lines can be detected through the thicket of night sky lines, and a much more diverse group of galaxies will be classified as “ $\mathcal{A}$ ” based on the presence of absorption lines in the 2500Å region.

Figure 2 gives illustrative examples of the five spectral classes used for extragalactic objects. The spectrum of the second brightest AGN and the second brightest starburst galaxy are shown, while for the other three spectral classes, the spectrum of the fifth brightest galaxy (at  $R$ ) assigned to that class is shown. The observed  $R$  magnitudes and  $z$  are indicated for each object. For the AGN and the spectral class “ $\mathcal{C}$ ” galaxy, the residuals from sky subtraction around the very strong night sky line at 5577Å were removed by interpolation. The “ $\mathcal{C}$ ” galaxy shown has a rather weak 3727Å emission line compared to most of the objects in this galaxy spectral class, but the distinction between “ $\mathcal{C}$ ” and “ $\mathcal{A}$ ” spectral classes is still clear from the relative strengths of absorption of H and K of CaII, the Balmer lines, and the molecular bands of CH and CN in this spectral region. The spectrum of a somewhat more typical higher- $z$  “ $\mathcal{C}$ ” galaxy is also shown for comparison.

As will be discussed in Cohen *et al.* (1998), there are many galaxies in this field with  $z \approx 0.58$ . At this redshift, the 3727Å emission line of [O II], a key spectral type diagnostic, is observed

at 5889Å, where it overlaps the strong NaD doublet in emission from the night sky. Unless the emission from such a galaxy at 3727Å [O II] is very strong, it may be lost in the uncertainty of subtracting away the much stronger night sky line. Thus, for this redshift only, the distinction between “A” and “C” spectral types has been made on the basis of the presence of the 3880Å CN band and the G band of CH at 4300Å. We assign such a galaxy a spectral class of “A” if those molecular bands are strong, while objects that show 4101Å H $\delta$  absorption in their spectra are assigned the spectral class “C”. A check of 19 objects originally classified as “A” in this redshift regime revealed three that had to be reclassified from “A” to “C” on this basis as well as three others too faint to determine which classification is most appropriate without the guidance of 3727Å emission, which were left as “A”.

For the brighter part of this sample with high precision spectra, considerably finer distinction among galaxy spectral classes is possible. A detailed discussion of the spectral features in the brighter galaxies of this sample is deferred to a future paper (Cohen et al 1999).

## 5. Redshifts for Objects in the Sample

Table 3 lists the object numbers, positions on the sky, measured  $K$  magnitudes (from Pahre *et al.* 1998), redshifts, spectral types, and quality classes for 195 objects in the main sample, followed by the 13 additional objects that constitute the total sample. Table 4 gives the distribution of objects in the main sample over the spectral and redshift quality classes.

Within the main sample, 84% of the objects have measured redshifts. The completeness is shown as a function of observed  $R$  and of observed  $K$  magnitude in Figure 3. As expected and supported by Figure 3, it is the  $R$  magnitude that primarily determines whether or not a redshift can be measured, rather than the  $K$  magnitude. The median  $R$  magnitude of the objects never observed is 24.6 mag, while the median  $R$  magnitude of the 21 objects that were observed, but for which no redshift was determined, is 24.3 mag. This latter group cannot contain any strong emission line objects with  $z < 1.1$  otherwise their spectra would have already yielded redshifts.

All of the objects with redshifts in the main sample have  $R$ ,  $I$  and  $K$  magnitudes from the data of Pahre *et al.* (1998), but several are too faint to be detected in the available  $U$ ,  $B$ , or  $V$  images.

The median redshift of the extragalactic objects in the main sample with measured  $z$  is 0.58. Even if it is assumed that all of the objects without redshifts are galaxies with  $z > 1$ , then the median redshift can only increase to  $z_{med} = 0.65$ . Table 5 presents the median redshift for the extragalactic objects in the main sample in half magnitude bins. The objects without redshifts have been ignored.

## 6. Summary

This paper provides a description of the techniques for analyzing and characterizing the spectra obtained by the Caltech Faint Galaxy Redshift Survey. We have given here the basic observational results of our spectroscopic investigation of a complete sample of objects with  $K_s < 20$  mag in a 2 by 7.3 arcmin field at J005325+1234. Redshifts were successfully obtained for 163 of the 195 objects in the sample using the LRIS at the Keck Observatory. An analysis of these data, combined with the six-color photometric data of Pahre *et al.*(1998), for the extragalactic objects in this field will be given in Cohen *et al.* (1998).

The entire Keck/LRIS user community owes a huge debt to Jerry Nelson, Gerry Smith, Bev Oke, and many other people who have worked to make the Keck Telescope and LRIS a reality. We are grateful to the W. M. Keck Foundation, and particularly its late president, Howard Keck, for the vision to fund the construction of the W. M. Keck Observatory. JGC is grateful for partial support from STScI/NASA grant AR-06337.12-94A. KR was supported in part by a Summer Undergraduate Research Fellowship at Caltech. RDB acknowledges support under NSF grant AST95-29170. DWH and MAP were supported in part by Hubble Fellowship grants HF-01093.01-97A and HF-01099.01-97A from STScI (which is operated by AURA under NASA contract NAS5-26555).

Table 1. Redshift Quality Classes

Quality Class	Description of Class
1	multiple features, $\sigma(z) \leq 0.002/\text{feature}$
2	multiple features, $\sigma(z) \leq 0.004/\text{feature}$
3	multiple features, faint, id uncertain, $\sigma(z)$ small 75% of time, and wildly off 25% of time
4	1 emission line only, solid, assume 3727Å
5	1 emission line only, reality uncertain, assume 3727Å
6	Multiple features, at least 1 broad emission line
7	Only 1 broad emission line, assumed to be 2800Å
8	Single break, assumed to be 4000Å break
9	Single strong absorption feature, assumed to be 2800Å because of shape of continuum
0	No redshift

Table 2. Definition of Spectral Types

Spectral Type	Defining Features
	Galactic Stars:
$\mathcal{M}$	TiO bands (M dwarfs); CaH bands (M subdwarfs)
$\mathcal{S}$	Absorption in Mg triplet, Balmer lines
$\mathcal{W}$	White dwarf, broad Balmer line absorption
	Extragalactic Objects:
$\mathcal{Q}$	At least one broad emission line
$\mathcal{B}$	Emission in $H\delta$ and $H\epsilon$ as well as 3727, $H\beta$ , 5007
$\mathcal{E}$	Dominated by emission lines, 3727, 5007
$\mathcal{C}$	composite, 3727 + Balmer line absorption
$\mathcal{A}$	No emission lines, only absorption features
	Unknown Objects:
$\mathcal{F}$	Observed, but no redshift
$\mathcal{U}$	Never observed spectroscopically

Table 3. Survey Objects

ID	RA <sup>1</sup>	Dec	K	z	QC	SC	ID	RA <sup>1</sup>	Dec	K	z	QC	SC
[D0K]	[-0 <sup>h</sup> ]	[-12 <sup>o</sup> ]	[mag]				[D0K]	[-0 <sup>h</sup> ]	[-12 <sup>o</sup> ]	[mag]			
1	5327.93	3018.40	12.73	0.000	1	$\mathcal{M}$	2	5327.69	3214.60	14.43	0.000	1	$\mathcal{S}$
3	5322.88	3546.60	14.91	0.000	1	$\mathcal{S}$	4	5322.94	3352.90	15.38	0.000	1	$\mathcal{M}$
5	5328.48	3717.70	15.58	0.000	1	$\mathcal{M}$	6	5328.72	3029.50	15.68	0.428	1	$\mathcal{A}$
7	5328.48	3731.40	15.87	0.000	1	$\mathcal{S}$	8	5327.87	3332.50	16.27	0.579	1	$\mathcal{A}$
9	5327.94	3613.70	16.30	0.441	1	$\mathcal{C}$	10	5325.61	3718.90	16.49	0.000	1	$\mathcal{M}$
11	5323.82	3729.90	16.67	0.346	1	$\mathcal{A}$	12	5324.73	3342.40	16.75	0.681	6	$\mathcal{Q}$
13	5324.12	3027.40	16.83	0.588	1	$\mathcal{C}$	14	5325.89	3536.90	16.88	0.428	1	$\mathcal{A}$
15	5324.55	3732.00	16.89	0.000	1	$\mathcal{M}$	16	5328.16	3044.40	16.95	0.431	1	$\mathcal{A}$
17	5322.22	3209.90	16.98	0.392	1	$\mathcal{A}$	18	5322.56	3252.30	17.02	0.173	1	$\mathcal{C}$
19	5325.95	3151.20	17.02	0.581	1	$\mathcal{A}$	20	5324.71	3437.80	17.10	0.000	1	$\mathcal{M}$
21	5327.85	3652.30	17.13	0.000	1	$\mathcal{M}$	22	5325.87	3144.90	17.14	0.581	1	$\mathcal{A}$
23	5323.46	3415.40	17.21	0.000	1	$\mathcal{M}$	24	5325.94	3423.30	17.30	0.679	1	$\mathcal{C}$
25	5324.24	3639.40	17.39	0.309	1	$\mathcal{C}$	26	5322.37	3059.00	17.44	1.115	6	$\mathcal{Q}$
27	5326.13	3147.80	17.44	0.577	1	$\mathcal{A}$	28	5324.43	3409.10	17.44	0.582	1	$\mathcal{A}$
29	5326.30	3239.20	17.45	0.582	1	$\mathcal{AC}$	30	5328.38	3501.80	17.52	0.621	1	$\mathcal{C}$
31	5329.12	3222.70	17.53	0.430	1	$\mathcal{A}$	32	5329.32	3330.10	17.54	0.577	1	$\mathcal{A}$
33	5325.91	3558.40	17.54	0.429	1	$\mathcal{A}$	34	5324.73	3411.80	17.55	0.679	1	$\mathcal{AC}$
35	5329.07	3457.20	17.56	0.428	1	$\mathcal{C}$	36	5323.73	3711.00	17.58	0.605	1	$\mathcal{AC}$
37	5326.88	3634.40	17.69	0.772	1	$\mathcal{A}$	38	5327.08	3610.40	17.75	0.763	1	$\mathcal{A}$
39	5323.21	3328.60	17.75	0.583	1	$\mathcal{C}$	40	5324.94	3202.30	17.80	0.582	1	$\mathcal{A}$
41	5322.00	3303.90	17.82	0.654	1	$\mathcal{AC}$	42	5327.65	3522.40	17.82	1.136	3	$\mathcal{A}$
43	5321.79	3018.00	17.86	0.000	1	$\mathcal{M}$	44	5321.92	3320.30	17.88	0.653	1	$\mathcal{C}$
45	5325.90	3158.70	17.88	0.581	1	$\mathcal{A}$	46	5325.50	3047.30	17.91	0.763	1	$\mathcal{C}$
47	5324.59	3347.00	17.99	0.582	1	$\mathcal{C}$	48	5327.76	3545.30	18.00	0.578	2	$\mathcal{C}$
49	5323.74	3441.70	18.06	0.584	1	$\mathcal{C}$	50	5323.10	3234.50	18.08	0.000	1	$\mathcal{M}$
51	5321.54	3135.40	18.09	0.677	1	$\mathcal{C}$	52	5327.78	3457.30	18.10	0.680	1	$\mathcal{C}$
53	5329.39	3307.20	18.10	0.000	1	$\mathcal{S}$	54	5328.49	3724.10	18.11	0.209	1	$\mathcal{EC}$
55	5324.02	3336.60	18.13	0.432	1	$\mathcal{C}$	56	5325.90	3229.60	18.27	0.689	3	$\mathcal{A}$
57	5327.08	3132.00	18.28	0.369	1	$\mathcal{EB}$	58	5328.86	3251.90	18.28	0.509	1	$\mathcal{C}$
59	5322.50	3549.70	18.29	0.771	1	$\mathcal{C}$	60	5329.13	3719.00	18.30	0.781	3	$\mathcal{A}$
61	5326.73	3650.20	18.32	0.000	1	$\mathcal{S}$	62	5327.54	3417.70	18.34	0.584	2	$\mathcal{A}$
63	5321.73	3141.00	18.35	0.535	3	$\mathcal{C}$	64	5324.50	3701.90	18.42	1.048	3	$\mathcal{A}$
65	5326.91	3051.30	18.44	1.232	3	$\mathcal{A}$	66	5325.60	3243.90	18.46	0.771	1	$\mathcal{EC}$
67	5327.95	3255.90	18.46	0.584	1	$\mathcal{A}$	68	5321.40	3153.70	18.47	1.392	2	$\mathcal{A}$
69	5321.32	3514.40	18.51	1.336	3	$\mathcal{A}$	70	5328.97	3156.00	18.54	0.581	1	$\mathcal{A}$
71	5323.70	3634.50	18.54	0.209	1	$\mathcal{E}$	72	5321.96	3341.10	18.56	...	0	$\mathcal{F}$
73	5326.51	3419.00	18.57	0.493	1	$\mathcal{C}$	74	5321.62	3117.90	18.60	0.676	2	$\mathcal{C}$
75	5322.20	3658.30	18.60	0.763	1	$\mathcal{C}$	76	5322.76	3155.00	18.63	1.153	6	$\mathcal{Q}$
77	5325.63	3510.80	18.64	...	0	$\mathcal{F}$	78	5329.70	3104.30	18.66	0.633	1	$\mathcal{B}$
79	5321.35	3346.80	18.68	0.533	1	$\mathcal{A}$	80	5325.68	3444.50	18.74	0.585	2	$\mathcal{C}$
81	5326.81	3030.10	18.75	0.414	1	$\mathcal{C}$	82	5323.64	3343.70	18.76	0.000	1	$\mathcal{M}$
83	5321.70	3426.30	18.80	0.429	1	$\mathcal{C}$	84	5326.45	3359.20	18.81	0.678	1	$\mathcal{C}$
85	5326.15	3350.40	18.81	0.626	1	$\mathcal{C}$	86	5324.44	3515.60	18.82	0.549	1	$\mathcal{E}$
87	5327.41	3308.50	18.82	0.440	1	$\mathcal{E}$	88	5327.26	3627.90	18.85	0.194	1	$\mathcal{E}$
89	5325.48	3108.40	18.86	0.581	1	$\mathcal{A}$	90	5328.99	3442.40	18.87	0.511	1	$\mathcal{C}$

Table 3—Continued

ID [D0K]	RA <sup>1</sup> [−0 <sup>h</sup> ]	Dec [−12°]	K [mag]	z	QC	SC	ID [D0K]	RA <sup>1</sup> [−0 <sup>h</sup> ]	Dec [−12°]	K [mag]	z	QC	SC
91	5324.24	3709.00	18.88	...	0	$\mathcal{F}$	92	5324.11	3645.90	18.89	0.000	1	$\mathcal{M}$
93	5322.02	3216.60	18.90	1.043	2	$\mathcal{A}$	94	5322.52	3732.00	18.91	...	0	$\mathcal{F}$
95	5326.78	3626.20	18.91	0.000	1	$\mathcal{M}$	96	5324.18	3020.20	18.94	0.677	1	$\mathcal{C}$
97	5328.80	3434.70	18.94	0.531	8	$\mathcal{A}$	98	5322.04	3045.50	18.97	...	0	$\mathcal{F}$
99	5324.95	3035.40	18.98	0.000	1	$\mathcal{M}$	100	5326.95	3552.90	19.00	0.680	2	$\mathcal{C}$
101	5325.93	3214.10	19.01	0.578	1	$\mathcal{A}$	102	5323.44	3336.00	19.01	0.448	3	$\mathcal{A}$
103	5321.72	3038.80	19.01	0.607	1	$\mathcal{EC}$	104	5323.46	3558.00	19.05	0.182	1	$\mathcal{B}$
105	5328.83	3334.80	19.05	0.681	1	$\mathcal{E}$	106	5322.29	3646.70	19.06	...	0	$\mathcal{U}$
107	5324.77	3148.00	19.10	...	0	$\mathcal{F}$	108	5328.14	3527.30	19.13	1.013	1	$\mathcal{E}$
109	5321.56	3607.60	19.15	0.000	1	$\mathcal{M}$	110	5327.24	3048.70	19.15	0.391	1	$\mathcal{E}$
111	5327.27	3136.90	19.17	0.582	1	$\mathcal{C}$	112	5324.19	3230.00	19.19	1.298	2	$\mathcal{EC}$
113	5326.12	3428.50	19.19	1.264	3	$\mathcal{A}$	114	5329.23	3447.00	19.21	0.583	1	$\mathcal{C}$
115	5327.94	3559.20	19.21	...	0	$\mathcal{F}$	116	5326.62	3432.50	19.24	0.584	1	$\mathcal{A}$
117	5328.22	3721.70	19.26	...	0	$\mathcal{F}$	118	5327.88	3429.80	19.27	...	0	$\mathcal{U}$
119	5326.11	3347.50	19.27	...	0	$\mathcal{F}$	120	5325.79	3125.60	19.27	...	0	$\mathcal{F}$
121	5325.47	3535.00	19.28	0.948	1	$\mathcal{E}$	122	5323.85	3413.40	19.30	0.570	2	$\mathcal{C}$
123	5322.47	3116.80	19.30	1.440	4	$\mathcal{E}$	124	5322.09	3037.40	19.30	...	0	$\mathcal{U}$
125	5323.10	3253.10	19.31	1.009	4	$\mathcal{E}$	126	5324.27	3017.20	19.31	1.301	5	$\mathcal{E}$
127	5323.24	3350.60	19.33	0.556	1	$\mathcal{B}$	128	5322.88	3551.10	19.34	1.307	3	$\mathcal{A}$
129	5329.21	3537.40	19.35	...	0	$\mathcal{U}$	130	5320.96	3318.20	19.35	...	0	$\mathcal{F}$
131	5323.83	3312.00	19.36	0.580	2	$\mathcal{C}$	132	5323.76	3215.40	19.36	0.391	1	$\mathcal{E}$
133	5323.64	3234.80	19.38	0.582	1	$\mathcal{C}$	134	5321.16	3120.10	19.39	0.000	1	$\mathcal{M}$
135	5324.48	3224.70	19.40	1.223	3	$\mathcal{A}$	136	5324.83	3430.40	19.40	...	0	$\mathcal{F}$
137	5323.66	3335.90	19.42	0.872	1	$\mathcal{EC}$	138	5322.55	3502.00	19.43	0.428	1	$\mathcal{C}$
139	5327.35	3245.10	19.43	0.573	3	$\mathcal{A}$	140	5328.40	3647.70	19.44	0.772	1	$\mathcal{C}$
141	5321.35	3124.30	19.45	...	0	$\mathcal{F}$	142	5322.40	3627.80	19.46	0.761	1	$\mathcal{A}$
143	5321.47	3319.80	19.47	0.750	3	$\mathcal{A}$	144	5323.55	3430.00	19.51	0.370	1	$\mathcal{E}$
145	5321.31	3158.60	19.51	0.581	1	$\mathcal{C}$	146	5329.14	3551.90	19.51	...	0	$\mathcal{F}$
147	5326.38	3116.20	19.52	0.415	1	$\mathcal{C}$	148	5328.79	3508.10	19.52	...	0	$\mathcal{U}$
149	5323.18	3711.10	19.53	0.269	1	$\mathcal{EB}$	150	5321.73	3724.30	19.53	0.862	3	$\mathcal{C}$
151	5322.98	3141.10	19.53	0.492	2	$\mathcal{C}$	152	5328.83	3103.40	19.55	1.075	9	$\mathcal{A}$
153	5326.38	3412.10	19.61	0.495	1	$\mathcal{C}$	154	5329.14	3542.20	19.62	...	0	$\mathcal{U}$
155	5321.35	3730.20	19.63	...	0	$\mathcal{F}$	156	5324.38	3241.30	19.63	...	0	$\mathcal{F}$
157	5323.71	3609.30	19.63	0.535	1	$\mathcal{C}$	158	5328.04	3140.90	19.65	1.306	1	$\mathcal{E}$
159	5321.43	3256.00	19.66	0.394	1	$\mathcal{E}$	160	5327.69	3607.30	19.68	0.000	1	$\mathcal{M}$
161	5324.43	3626.70	19.70	0.432	1	$\mathcal{C}$	162	5322.76	3644.80	19.71	0.643	1	$\mathcal{C}$
163	5324.72	3356.00	19.72	0.580	3	$\mathcal{A}$	164	5328.66	3139.30	19.72	0.587	2	$\mathcal{C}$
165	5328.48	3056.80	19.73	0.581	8	$\mathcal{A}$	166	5326.60	3547.70	19.74	0.611	1	$\mathcal{EC}$
167	5329.19	3351.70	19.74	0.442	1	$\mathcal{C}$	168	5321.60	3204.00	19.74	...	0	$\mathcal{U}$
169	5325.51	3530.70	19.76	...	0	$\mathcal{F}$	170	5322.02	3547.60	19.76	0.533	1	$\mathcal{E}$
171	5326.33	3020.90	19.77	0.345	1	$\mathcal{E}$	172	5322.74	3209.00	19.77	0.974	9	$\mathcal{A}$
173	5321.11	3243.50	19.81	...	0	$\mathcal{U}$	174	5325.24	3640.70	19.83	0.968	5	$\mathcal{E}$
175	5325.66	3434.70	19.84	0.939	4	$\mathcal{E}$	176	5324.05	3536.10	19.85	...	0	$\mathcal{F}$
177	5325.52	3559.00	19.86	...	0	$\mathcal{U}$	178	5326.15	3359.60	19.88	0.745	3	$\mathcal{A}$
179	5328.56	3618.20	19.89	0.763	2	$\mathcal{C}$	180	5322.23	3650.60	19.90	...	0	$\mathcal{F}$

Table 3—Continued

ID [D0K]	RA <sup>1</sup> [−0 <sup>h</sup> ]	Dec [−12°]	K [mag]	z	QC	SC	ID [D0K]	RA <sup>1</sup> [−0 <sup>h</sup> ]	Dec [−12°]	K [mag]	z	QC	SC
181	5324.83	3254.70	19.91	1.040	9	$\mathcal{A}$	182	5323.55	3357.60	19.92	1.137	3	$\mathcal{A}$
183	5323.03	3437.60	19.92	0.922	1	$\mathcal{E}$	184	5322.63	3509.80	19.92	0.622	1	$\mathcal{C}$
185	5327.51	3611.40	19.92	0.975	1	$\mathcal{E}$	186	5321.63	3020.50	19.95	...	0	$\mathcal{U}$
187	5324.24	3630.60	19.96	0.344	1	$\mathcal{C}$	188	5324.47	3617.90	19.98	1.218	2	$\mathcal{A}$
189	5321.69	3303.70	19.98	0.490	4	$\mathcal{A}$	450	5329.09	3030.30	18.12	0.000	1	$\mathcal{M}$
956	5325.20	3615.60	19.48	0.000	1	$\mathcal{M}$	494	5326.02	3534.90	18.91	...	0	$\mathcal{F}$
504	5322.56	3252.30	19.06	...	0	$\mathcal{F}$	506	5322.88	3546.60	19.07	...	0	$\mathcal{U}$
507	5324.73	3408.00	19.12	1.002	4	$\mathcal{E}$							
Supplemental objects													
451	5322.12	3354.90	20.65	0.430	8	$\mathcal{A}$	951	5329.56	3644.50	-20.00	0.440	1	$\mathcal{C}$
953	5330.64	3632.40	-20.00	0.280	1	$\mathcal{E}$	958	5327.06	3546.90	20.02	0.442	1	$\mathcal{C}$
961	5318.41	3516.40	-20.00	0.000	1	$\mathcal{S}$	968	5324.21	3325.70	20.58	0.000	1	$\mathcal{S}$
971	5331.26	3212.00	-20.00	0.352	1	$\mathcal{E}$	973	5330.40	3041.00	-20.00	0.340	1	$\mathcal{E}$
980	5326.00	3157.01	20.20	0.437	1	$\mathcal{E}$	982	5329.11	3020.81	20.45	1.420	9	$\mathcal{A}$
983	5325.62	3504.53	-20.00	0.460	8	$\mathcal{A}$	984	5321.50	3123.00	20.60	1.119	1	$\mathcal{E}$
985	5321.16	3004.50	-20.00	0.773	4	$\mathcal{E}$							

<sup>1</sup>ID, RA, Dec, and R magnitude from Pahre *et al.* 1998.

Note. — QC is the quality code described in §3.3. SC is the spectral classification described in §4.

Table 4. Distribution of Sample Among Galaxy Spectral Types and Quality Classes

Spectral Class	No. of Objects	Quality Class	No. of Objects
$\mathcal{M}$	19	1	117 <sup>1</sup>
$\mathcal{S}$	5	2	14
$\mathcal{Q}$	3	3	17
$\mathcal{B}$	3	4	5
$\mathcal{E}$	30	5	2
$\mathcal{C}$	50	6	3
$\mathcal{A}$	53	7	0
$\mathcal{F}$	21	8	2
$\mathcal{U}$	11	9	3
		0	32

<sup>1</sup>Includes 24 Galactic stars.

Table 5. Median Redshift with Magnitude

magnitude bin	$R$		$K$	
	$N$	$\langle z \rangle$	$N$	$\langle z \rangle$
15.5-16.0	0		1	0.43
16.0-16.5	0		2	0.44
16.5-17.0	0		6	0.43
17.0-17.5	0		9	0.58
17.5-18.0	0		18	0.58
18.0-18.5	0		17	0.58
18.5-19.0	1	0.68	23	0.58
19.0-19.5	2	0.17	30	0.61
19.5-20.0	1	0.31	33	0.58
20.0-20.5	7	0.43		
20.5-21.0	4	0.43		
21.0-21.5	23	0.44		
21.5-22.0	23	0.58		
22.0-22.5	21	0.58		
22.5-23.0	28	0.64		
23.0-23.5	20	0.86		
23.5-24.0	5	0.76		
24.0-24.5	4	0.75		

## REFERENCES

- Bruzual, G., & Charlot, S. 1993, *ApJ*, 405, 538
- Cohen, J. G. *et al.* 1999, in preparation
- Cohen, J. G., Blandford, R., Hogg, D.W., Pahre, M.A. & Shopbell, P.L., 1998, submitted to the *ApJ*
- Colless, M., & Boyle, B. 1998, in *Highlights in Astronomy*, 11, in press (astro-ph/9710268)
- Cowie, L. L., Hu, E. M., & Songaila, A. 1995, *Nature*, 377, 603
- Cowie, L. L., Songaila, A., Hu, E. M., & Cohen, J.G. 1996, *AJ*, 112, 839
- Dey, A., Spinrad, H., Stern, D., Graham, J. R., & Chaffee, F. H., 1998, *ApJ*, 498, L93
- Ellis, R. S., Colless, M., Broadhurst, T., Heyl, J. & Glazebrook, K. 1996, *MNRAS*, 280, 235
- Ellis, R. S. 1997, *ARA&A*, 35, 389
- Fanelli, M.N., O'Connell, R.W., Burstein, D. & Wu, C.C., 1992, *ApJS*, 82, 197
- Francis, P. J., Hewett, P. C., Foltz, C. B., Chaffee, F. H., Weymann, R. J., & Morris, S. L. 1991, *ApJ*, 373, 465
- Geller, M. J., Kurtz, M. J., Wegner, G., Thorstensen, J. R., Fabricant, D. G., Marzke, R. O., Huchra, J. P., Schild, R. E., & Falco, E. E., 1997, *AJ*, 114, 2205
- Glazebrook, K., Offer, A. R., & Deeley, K. 1998, *ApJ*, 492, 98
- Griffiths, R. E. *et al.* 1994, *ApJ*, 435, L19
- Gunn, J. E., & Knapp, G. R. 1993, in *Sky Surveys: Protostars to Protogalaxies*, ed B. T. Soifer, (ASP Conference Series), 267
- Huchra, J. P., Davis, M., Latham, D., & Tonry, J. 1983, *ApJS*, 52, 39
- Kurtz, M. J., & Mink, D. J.. 1998, submitted to *PASP*
- Koo, D. C., 1998, in *Redshift Surveys of the 21st Century*, ed. A. Fairall (Kluwer: Dordrecht), in press
- Koo, D. C., & Kron, R. G. 1992, *ARA&A*, 30, 613
- Lilly, S. J., LeFèvre, O., Crampton, D., Hammer, F. & Tresse, L. 1995a, *ApJ*, 455, 50
- Lilly, S. J., Hammer, F., LeFèvre, O., & Crampton, D., 1995b, *ApJ*, 455, 75
- Madau, P., Pozzetti, L., & Dickinson, M. 1998, *ApJ*, 498, 106

Oke, J. B. 1990, *AJ*, 99, 1621

Oke, J. B., Cohen, J. G., Carr, M., Cromer, J., Dingizian, A., Harris, F. H., Labrecque, S.,  
Lucinio, R., Schaal, W., Epps, H., & Miller, J. 1995, *PASP*, 107, 307

Pahre, M. A., *et al.* 1998, *ApJS*, submitted

Shectman, S.A., Landy, S. D., Oemler, A., Jr., Tucker, D. L., Lin, H. A., Kirshner, R. P., &  
Schechter, P. L. 1996, *ApJ*, 470, 172

Shortridge, K. 1988, “The Figaro Manual Version 2.4”

Skrutskie, M. *et al.* 1999, “2MASS Explanatory Supplement”, in preparation

Steidel, C. C., Giavalisco, M., Pettini, M., Dickinson, M., & Adelberger, K. L. 1996, *ApJ*, 462, L17

Vettolani, G., *et al.* 1997 *A&A*, 325, 954

Wainscoat, R. J., & Cowie, L. L. 1992, *AJ*, 103, 332

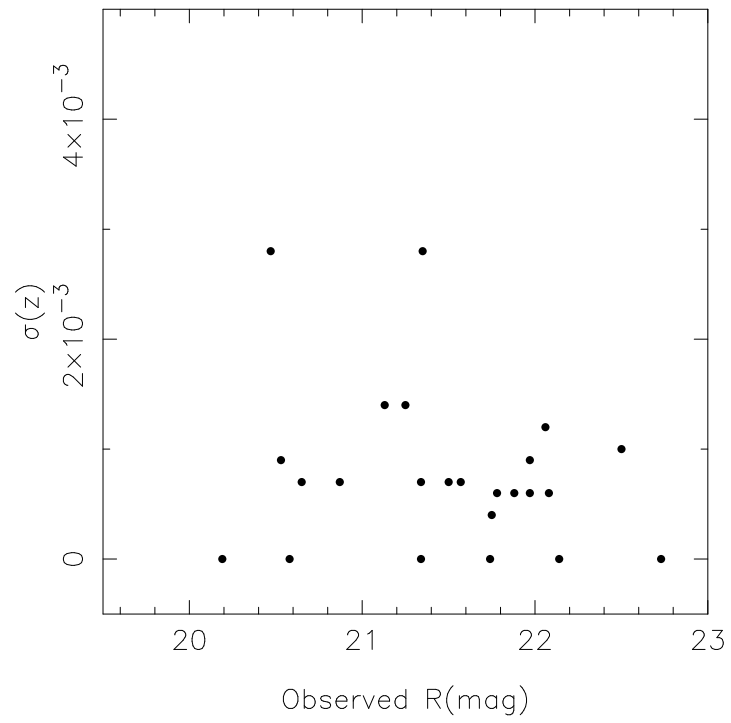


Fig. 1.— The rms dispersion in redshift is shown for galaxies with multiple spectra as a function of  $R$  magnitude. The implied scatter for a single redshift measurement is  $\sim 0.0008$ .



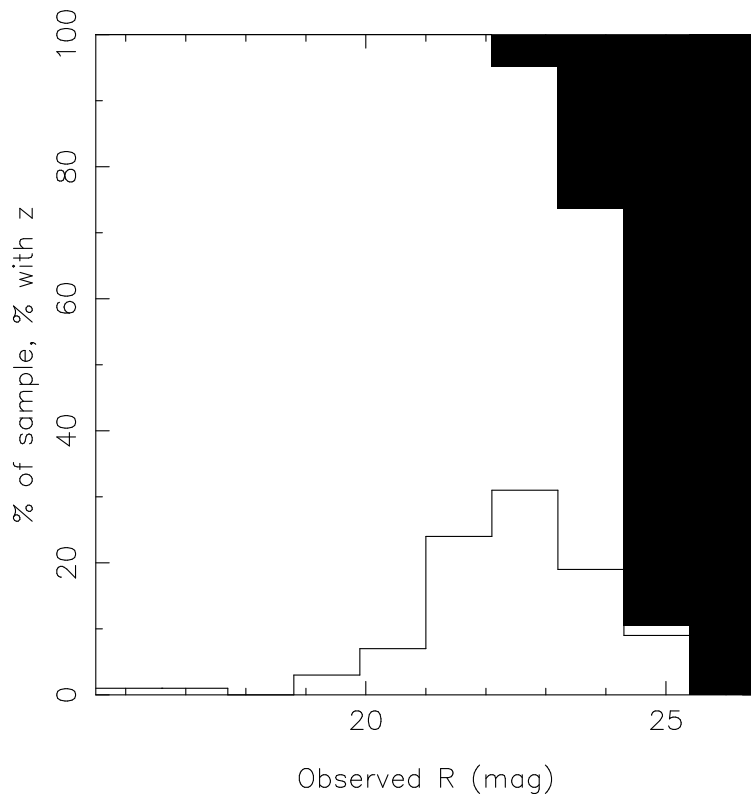
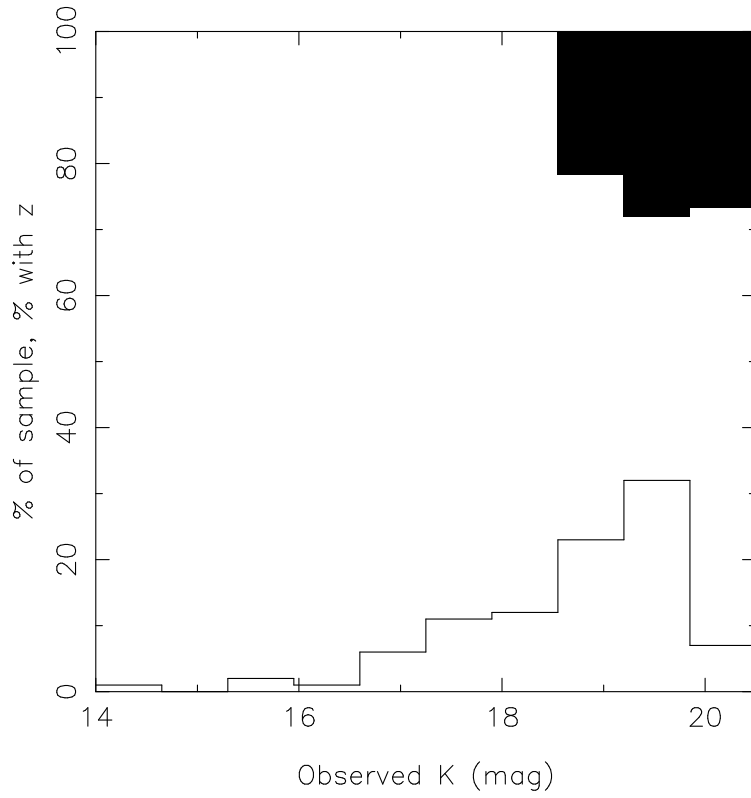


Fig. 3.— A histogram of the sample and the completeness of the redshifts are shown for the main sample. The filled area denotes the objects without redshifts. Figure 3a displays this for the  $K$  filter, while figure 3b show the results using the  $R$  filter.